Topics in Catalysis
https://doi.org/10.1007/s11244-022-01763-7

ORIGINAL PAPER

Copper-zeolites Prepared by Solid-state Ion Exchange - Characterization and Evaluation for the Direct Conversion of Methane to Methanol

Karoline Kvande[1] · Sebastian Prodinger[1] · Fabian Schlimpen[2] · Pablo Beato[3] · Patrick Pale[2] · Stefan Chassaing[2] · Stian Svelle[1]

Accepted: 5 December 2022

Abstract
Direct conversion of methane to methanol (MTM) over Cu-zeolites is a so-called "dream reaction" for the chemical industry. There is still a lot that can be done in order to optimize the reaction by e.g. achieving a deeper understanding of the reaction mechanism and the nature of the Cu-sites. In this study, we investigated a solid-state ion exchange method to incorporate Cu^{I} ions into zeolites (MOR, BEA, ZSM-5 and FAU), as a more scalable technique. The solid-state ion exchange led to a Cu/Al ration of about 0.8, however with a heterogeneous distribution of Cu. Regardless, Fourier transform-infrared spectroscopy still revealed that most Brønsted acid sites were exchanged in all four samples. Further, CH_4-temperature programmed reaction experiments showed that some Cu-sites formed were reactive towards CH_4, with Cu^{I}-MOR and Cu^{I}-FAU having the largest CH_4 consumption. Ultimately, the Cu^{I}-zeolites were tested in the MTM reaction and proved capable of producing methanol, even without the presence of Brønsted sites. A MOR with lower Cu/Al ratio (0.30) was also tested for comparison, and as this sample obtained a much higher productivity than the Cu^{I}-MOR with high Cu-loading (0.10 vs. 0.03 mol_{MeOH}/mol_{Cu}), it was demonstrated that some fine-tuning is necessary to obtain the active Cu sites for methane activation.

Keywords Methane activation · Solid-state ion exchange · Cu^{I} –zeolites

1 Introduction

A lot of research effort has been dedicated over the last decades to find a small-scale conversion route for underutilized methane, due to its potential impact on climate change mitigations. The direct conversion of methane to methanol (MTM) is one of the highly explored research areas related to this. Several different reaction routes have been proposed for this, although one of the more promising ones is a stepwise cyclic conversion route over metal-loaded zeolites, and especially Cu-zeolites. This is because the stepwise cyclic conversion route facilitates for the separation of product and oxidant to prevent over-oxidation [1–3]. This method includes a high temperature (~500°C) oxidation step of the Cu-zeolite in O_2 before the temperature is reduced to 200 °C and the resulting material is then reacted with CH_4. This reduces some of the Cu-oxo sites (mono- and dimeric Cu moieties) formed after O_2-activation, and methoxy intermediates are formed on these sites. Finally, steam is required to extract methanol from the zeolite pores. On the quest of optimizing the reaction, a large array of Cu-zeolites have been investigated. Among the most investigated are MOR [4–6], CHA [7, 8], and ZSM-5 [9, 10]. MOR has been found to be one of the most active zeolites with methanol productivities close to 0.5 mol_{MeOH}/mol_{Cu} [11, 12]. This is often viewed to be the highest obtainable productivity, given a Cu

✉ Karoline Kvande
karoline.kvande@smn.uio.no

[1] Center for Materials Science and Nanotechnology (SMN), Department of Chemistry, University of Oslo, 1033 Blindern, 0315 Oslo, Norway

[2] Laboratoire de Synthèse, Réactivité Organiques et Catalyse (LASYROC), Institut de Chimie, CNRS-UMR7177, Université de Strasbourg, 4 rue Blaise Pascal, 67070 Strasbourg, France

[3] Topsoe A/S, Haldor Topsøes Allé 1, DK-2800 Kgs. Lyngby, Denmark

Published online: 27 December 2022

to methanol ratio of two-to-one [13, 14]. This ratio is based on the active site being a dicopper active site (Cu-O-Cu or Cu-O-O-Cu), or the combination of two monomeric sites (Cu-OH) [11, 15]. It has been found that both the zeolite framework and placement of Cu have large impacts on the formation of the active sites and as a consequence, the activity towards methanol formation [12]. Therefore, finding new materials and synthesis methods is still very important in the attempts to optimize the MTM process. In literature, the Cu loading into zeolites is mostly performed *via* liquid ion exchange or incipient wetness methods with Cu^{II} salts, both giving well-dispersed Cu-zeolites, however only in lab scale quantities [4, 16]. For industrial application, it would be much more beneficial to use a simpler exchange method like solid-state ion exchange (SSIE). SSIE is also relevant for the selective catalytic reduction of NO_x with NH_3, and to that end, Vennestrøm and Shwan et al. have previously investigated a novel method to perform SSIE with CuO/Cu_2O in an atmosphere of NO/NH_3 [17, 18]. Therein, they suggest that the Cu-oxo species are formed at low temperatures due to the formation of mobile $[Cu(NH_3)_2]^+$ complexes.

In this study, we have prepared Cu^I exchanged zeolites *via* SSIE with Cu^ICl (Cu^I-BEA, -FAU, -MOR and -ZSM-5) and tested the materials in the methane to methanol reaction. Le et al. have previously shown that SSIE with $Cu^{II}(acac)_2$ instead of Cu^ICl over mordenites lead to a higher yield of methanol [19]. However, when exchanging Cu^I ions instead of Cu^{II} ions into the zeolites, it is theoretically possible to obtain a Cu/Al = 1, thus maximizing the possible Cu-oxo sites. A similar protocol using SSIE with Cu^ICl to exchange H-mordenites for the MTM reaction was previously applied by Bozbag et al., however, they did not explore the possibility of fully exchanging the materials, and used Cu/Al ratios around 0.35 [20]. The SSIE method discussed in this study have also been used to synthesise Cu^I-exchanged FAU zeolites that have been investigated as a catalyst for C–C bond Glaser-type homocoupling reactions by Kuhn et al. [21]. Furthermore, the Cu ^{I}-FAU zeolite has been shown to be applicable as a catalyst in several other types of organic synthesis [22–26]. This truly shows the adversity of Cu-sites in zeolites. To fully study the effect of this SSIE synthesis method for the MTM reaction, the samples were subjected to elemental analysis, and investigated with CO-adsorption coupled with Fourier Transform-Infrared (FT-IR) spectroscopy to understand if the increased amount of Cu led to changes in the Cu speciation. Furthermore, CH_4-TPR experiments, shown to be a helpful tool in optimizing the MTM reaction both in terms of setting the reaction parameters as well as understanding material properties, were performed [27, 28]. Finally, the samples were tested in the methane to methanol reaction and compared to previously obtained results with the same reaction protocol in order to assess their performance. The target with this investigation is to understand whether it is possible to form methanol from methane when most Brønsted sites are exchanged with Cu, or if this alters the properties of the Cu-sites to an extent where C-H activation is no longer possible. Further, we also aim to clarify the importance of minimizing the formation of Cu agglomerates and nanoparticles to obtain a high methanol productivity.

2 Methods

2.1 Solid-state Cu-exchange

The four zeolite materials used as starting material in this study were commercially available and received in the NH_4-form. The four zeolite frameworks were FAU (USY) zeolite (Zeolyst International (CBV500), Si/Al = 2.9), MOR zeolite (CBV21A, Si/Al = 10.3), BEA zeolite (Zeochem International (ZEOCAT PB/H), Si/Al = 12.5–17.5) and ZSM-5 zeolite (Zeolyst International (CBV5020), Si/Al = 25). The H-form was obtained by calcining the NH_4-form for 12 h at 550 °C in static air. To obtain the expected Cu^I-exchanged forms of the samples, a solid-state ion exchange was performed by mixing 1 g of dry zeolite with a calculated amount of CuCl (Aldrich, > 99% purity, melting point: 430 °C) to obtain a specific Cu/Al ratio, where the Cu exchange degree was about 80%. The samples were named Cu^I-FAU, Cu^I-MOR, Cu^I-BEA, and Cu^I-ZSM-5. All samples were made with an intended Cu/Al ratio ≈ 0.8. One Cu-MOR was made with a lower Cu/Al ratio (~0.30) for comparison. This was named $0.30Cu^I$-MOR. To limit the exposure to moisture, the mixture was rapidly ground with a mortar and pestle before being loaded into a tubular reactor and connected to a flow setup. The powder mixture was heated to 350 °C (1 °C/min) and held isothermally for 3 d. N_2 was used as a purging gas (40 ml/min) to remove the gaseous HCl formed during the reaction.

2.2 Standard characterization

Microwave Plasma Atomic Emission Spectroscopy (MP-AES) was used for elemental analysis of the sample. Before analysis, 20 mg of sample was dissolved in 1 mL 15% hydrofluoric acid (HF) in a Teflon liner for 1 h. Safety note: The use of hydrofluoric acid requires special precautions. To verify that all of the solid material was dissolved, a light was shone through the thin wall of the Teflon liner. After quenching excess fluoride anions by adding an appropriate amount of 5 wt% H_3BO_3, the solution was diluted with distilled water (50 mL). An Agilent 4100 MP-AES instrument

was used to analyze the solution, and the amount of Si, Al and Cu in µmol/g was quantified with external calibration curves based on commercial elemental standards.

Scanning Electron Microscopy (SEM) combined with backscattered electron (BSE) imaging was used to investigate the samples for Cu nanoparticles before and after activity testing. A Hitachi SU8230 microscope was used to obtain the images using an acceleration voltage of 1 kV and a 10 µA current. On the same instrument, Energy Dispersive X-ray (EDX) was used as a secondary elemental analysis to determine the ratio of Cl in the sample in relation to the Cu content before and after testing. The distribution of Cu on the sample was investigated with EDX mapping.

Thermogravimetric Analysis (TGA) was used to measure the water content (in %) of the samples. For this, a Netzsch STA 449 F Jupiter system was applied to measure the sample weight. The materials were heated to 300 °C with a ramp rate of 2 °C/min in a flow of synthetic air (20 ml/min O_2 and 40 ml/min N_2).

X-ray Diffraction (XRD) patterns of the tested materials were obtained using a Bruker D8 Discovery diffractometer with a Cu Kα radiation (λ = 1.5418 Å). The materials were grinded, and evenly dispersed to make a flat surface on a glass plate sample holder. The experiments were run in a 2θ range of 2–50° with a step size of 0.02 °/s at ambient conditions.

N_2-physisorption isotherms was used to determine the specific surface area of the samples. The measurements were conducted on a BELSorp Maxi volumetric gas adsorption instrument (MicroTrac MRB) at − 196 °C. The samples were pretreated by evacuation at 300 °C for 10 h. The specific surface areas were calculated by using the BET approximation in a p/p_0 range relevant for microporous materials as defined by Llewellyn et al. [29].

2.3 CO-adsorption with Fourier transform-infrared (FT-IR) spectroscopy

For the CO-adsorption FT-IR experiments, the samples were pressed (2–3 tons) into thin wafers (~11.3 mg/cm^2) and carefully placed into gold envelopes. Then the gold envelope was placed into a T-shaped cell with KBr windows. The cell was connected to vacuum and pretreated at 450 °C for 90 min after a ramp of 5 °C/min from room temperature (RT). After cooling back down to RT, the setup was placed into a Bruker Vertex 80 FT-IR instrument and incremental doses of CO was sent onto the sample until reaching an equilibrium pressure of ~8 mbar. A spectrum was collected after each dose.

2.4 Activity measurements in the methane to methanol reaction

All samples were tested in the methane to methanol reaction. 100 mg of sample (sieve fraction: 425 – 250 µm) were loaded into a linear quartz reactor (i.d. = 6 mm) and then connected to a gas manifold controlled by Mass Flow Controllers (MFC). The gas feeds were sent stepwise onto the sample, controlled by stop- and 4-way valves. Water was connected to the gas line through a bubbler immersed in an oil bath kept at 45 °C. All gas lines were heated to ~140 °C to avoid any condensation in the lines. The effluent was analyzed with an online Pfeiffer Mass Spectrometer after the reactor. All gas flows were adjusted to 15 mL/min, using a flow meter. In a flow of 100 O_2, the sample was heated to 500 °C (5 °C/min) and kept there for 8 h. Then the temperature was reduced to 200 °C, and 100 He was used to flush out excess O_2 for 1 h. After that, a flow with 100 CH_4, was sent onto the sample for 3 h. Another round with He flush for 1 h was performed, before a 10 H_2O saturated 10 Ne/He stream was sent onto the sample for 2 h. The mass fragments of MeOH (m/z = 31), DME (m/z = 46) and CO_2 (m/z = 44) was quantified using calibration curves from obtained using a calibration gas mixture with known amounts of all the components. To obtain the accurate yield, the sample weight was corrected by withdrawing the water content of the samples (measured with TGA). The total yield (µmol/$g_{zeolite}$) of MeOH is given as the amount of MeOH + 2 ~ DME. In the text this will be referred to as *total amount of methanol*.

2.5 CH_4-Temperature programmed reaction (TPR)

For the CH_4-TPR experiments, the same setup as for testing was used. After pretreating the samples in O_2 in the same manner as above, the temperature was lowered to 105 °C, and He was sent onto the sample to flush away all excess O_2 for 1 h. Then 15 mL/min 5% CH_4/He was sent onto the sample for 20 min isothermally, before a ramp up to 550 °C with 5 °C/min was started. The temperature was recorded simultaneously with a thermocouple placed in a thin quartz sheet on top of the sample bed. The output of the reactor was analyzed with an online MS.

3 Results and Discussion

3.1 Basic characterization by MP-AES, EDX, SEM, XRD and N_2-physisorption

Solid state ion exchange (SSIE) is industrially a much simpler synthesis process than various solution-based exchange procedures. Furthermore, by performing the SSIE with Cu^I

Table 1 Chemical composition of the materials obtained with Microwave Plasma Atomic Emission Spectroscopy (MP-AES).

Sample name	Si/Al	Cu/Al	Al wt%	Al (mmol/g)	Cu wt%	Cu (mmol/g)
Cu^{I}-ZSM-5	18.4	0.78	2.3	0.86	4.2	0.67
Cu^{I}-BEA	35.7	2.0	1.2	0.45	5.9	0.92
Cu^{I}-MOR	12.0	0.89	3.5	1.3	7.2	1.1
Cu^{I}-USY	2.9	0.74	12	4.3	20	3.2
0.30Cu^{I}-MOR	11.8	0.31	3.5	1.3	2.5	0.40

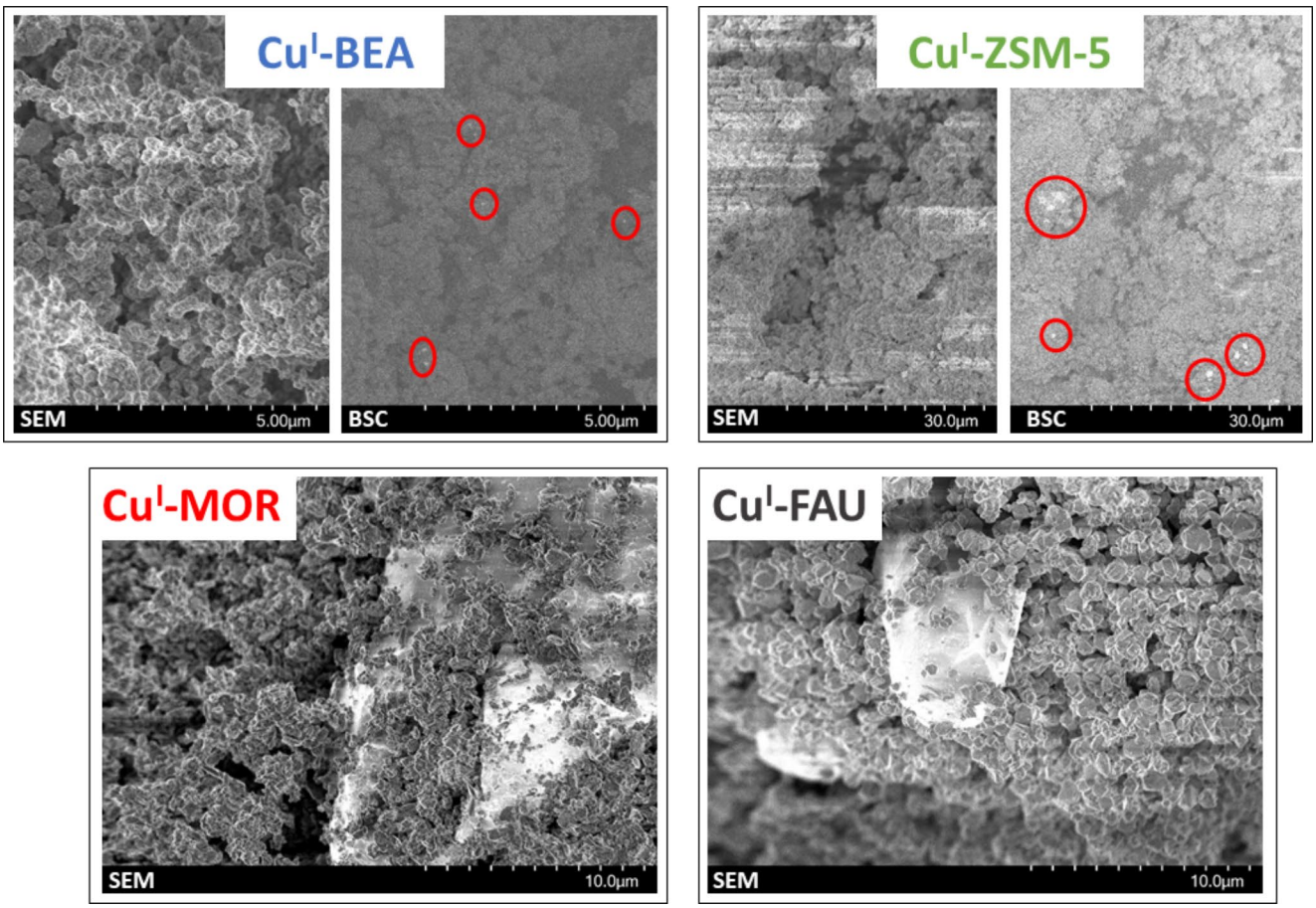

Fig. 1 SEM and Backscatter (BSC) images of the materials. The top row shows the presence of nanoparticles observed with Backscattering imaging (bright spots in the red circles). Bottom row shows larger agglomerates visible in regular SEM images

salts, it would be possible to obtain a higher exchange degree of Cu in the zeolite, possibly leading to a larger concentration of copper in close proximity. Their close proximity could make the formation of active sites for C-H activation more feasible. To investigate the resulting Cu-zeolites after SSIE, MP-AES and EDX was used for elemental analysis, N_2-physisorption was applied to determine the specific surface area, and SEM and backscattered images was used to search for Cu outside the frameworks. A more extensive characterization on the effect of the SSIE has been performed on the Cu^{I}-exchanged FAU sample previously by Kuhn et al. [21]. For three of the zeolites, the SSIE yielded Cu-loaded zeolites with a molar Cu/Al ratio ≈ 0.8. Cu^{I}-BEA ended up over-exchanged with a Cu/Al = 2, due to the much lower Al content than indicated by the manufacturer in this sample. A full report on the elemental analysis from MP-AES is presented in Table 1.

Figure 1 depicts the SEM and backscattered electron images obtained for the four samples. In Cu^{I}-BEA and Cu^{I}-ZSM-5, Cu nanoparticles can be observed as bright spots in the backscattered electron images, as pointed out by the red circles. In the regular SEM images of Cu^{I}-MOR and Cu^{I}-FAU, even larger agglomerates of Cu are observed. This was also corroborated with EDX mapping, which showed big agglomerates of Cu outside the framework (Fig. S1). These images indicate a very heterogeneous distribution of Cu in the materials and demonstrates the possible drawback of SSIE as exchange procedure.

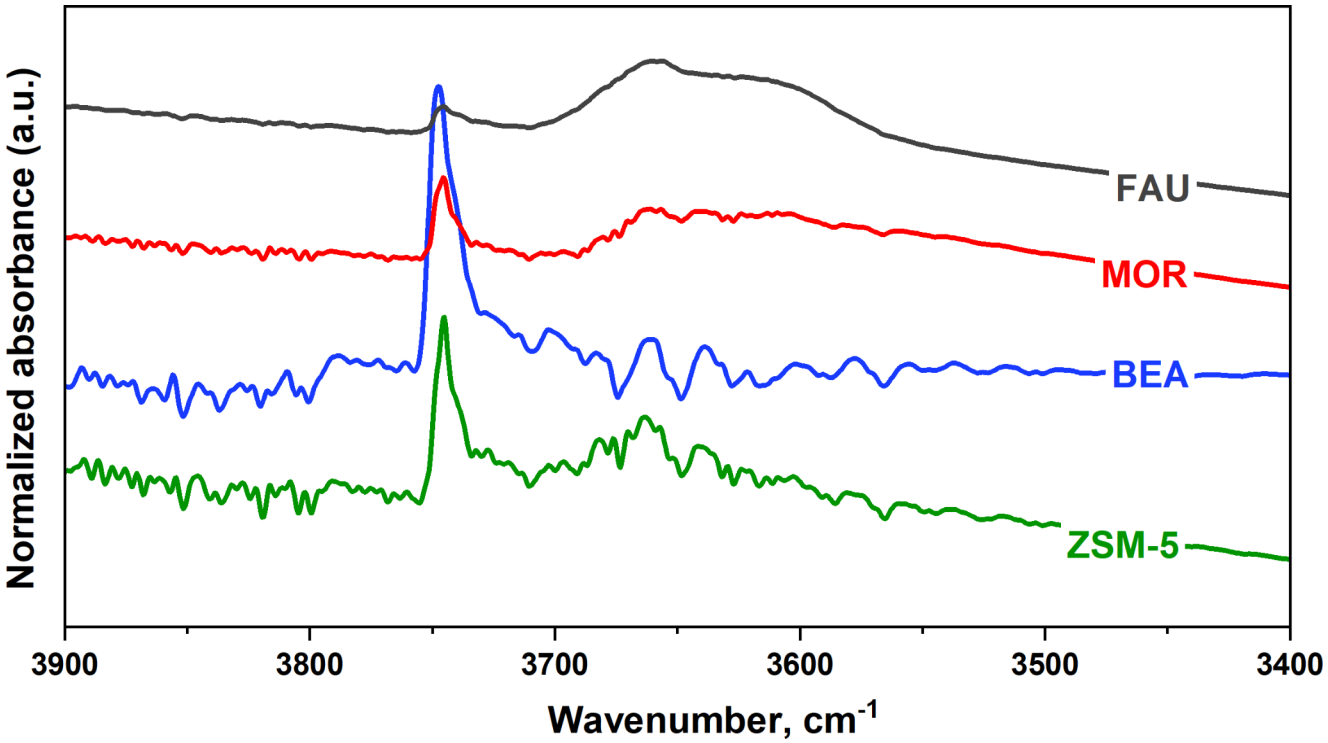

Fig. 2 FT-IR spectra showing the ν(OH) stretching region of the four Cu^{I}-zeolites after pretreatment in vacuum at 450 °C

In addition to the heterogeneous distribution of Cu, elemental analysis with EDX revealed that a significant fraction of Cl was found in all samples as a remnant from the SSIE.

The specific surface area of all samples were obtained using N_2-physisorption, and compared to the specific surface area of the H-form (Table S1). It is apparent that there is a reduction in surface area (> 10%) for most of the samples after the Cu exchange. This loss in surface area could indicate that the formation of nanoparticles and the large excess of Cu contributes to a partial pore blockage for reactants. This is substantiated by the specific surface area of the MOR sample with a smaller Cu/Al ratio, $0.30Cu^{I}$-MOR being much higher than for the higher Cu-loaded Cu^{I}-MOR sample.

XRD of the as-synthesized FAU has previously shown that the framework is intact after the Cu exchange and HCl release [21]. Herein, we have measured the XRD pattern of the tested samples. The patterns are presented in Fig. S2. The patterns obtained indicate that $0.30Cu^{I}$-MOR, Cu^{I}-MOR, Cu^{I}-ZSM-5 and Cu^{I}-FAU has kept the structural integrity after testing. However, it should be noted that impurities of both $CuCl_2$ and CuO was present in the highly exchanged samples, as evidenced by some additional peaks at $2\theta = 16$, 32 and 40°.

The basic characterization of the solid-state ion exchanged materials reveal that there is a heterogeneous distribution of Cu in the samples and possible pore blockage by larger agglomerates present around the pores. Therefore, even though the exchange led to a Cu/Al ratio of 0.8, it is not likely that all the Cu present in the samples will contribute to C-H bond activation.

3.2 CO-adsorption with FT-IR spectroscopy

The effects of the very high exchange degree achieved for the four zeolites (Cu/Al ratio of 0.8) on Cu speciation were studied using FT-IR spectroscopy. Figure 2 depicts the ν(OH) stretching region of the spectra at RT after pretreatment at 450 °C in vacuum. O-H stretching bands connected to Brønsted sites (Si(-OH)Al) should be found in the region between 3700 and 3550 cm^{-1}. The lack of bands in this region indicates that all Brønsted sites are covered by Cu, except a broad band in the Cu^{I}-FAU sample. A comparison between the parent MOR and the Cu-exchanged MOR for this region can be found in the SI (Fig. S3). The bands at ~3750 cm^{-1} are related to silanols (Si-OH) in the samples. The non-existing Brønsted site vibrations should be noted, as it has been previously suggested that Brønsted sites are necessary to produce methanol, as shown with the help of FT-IR and NMR spectroscopy by Dyballa et al. as well as Sushkevich et al. [30, 31]. The effect of the lacking Brønsted sites on the performance of the materials will be discussed in-depth later in this paper.

Dosing CO at RT onto the pretreated materials can determine if the high Cu/Al ratio has an impact on the nature of

the Cu-sites and their accessibility. CO will only form stable adducts with Cu^{I} ions and not Cu^{II} ions at RT. Therefore, ideal conditions would be to ensure that all Cu ions in available, redox active sites, are oxidation state 1+, and hence able to react with CO. To do so, the Cu^{I}-exchanged samples were pretreated at 450 °C under vacuum prior to the CO-adsorption measurements, as this has been shown to induce "self-reduction" of Cu^{II} to Cu^{I} in zeolites [32–36].

In Fig. 3, IR absorption spectra of all four samples during CO adsorption is shown. The background subtracted spectra have been normalized to the sample weight. The last spectra in all four series is recorded at ~8 mbar equilibrium CO pressure. These precautions ensure a fair comparison when discussing the band intensities of the four samples. As the samples are exposed to incremental doses of CO, the bands typical for mono- and eventually dicarbonyl adducts on Cu^{I} sites will be formed [37]. The band(s) related to the formation of monocarbonyl species are highlighted with a grey background. This appears as a growing band at 2158 and 2157 cm^{-1} for Cu^{I}-MOR and Cu^{I}-ZSM-5, while for Cu^{I}-FAU and Cu^{I}-BEA, the monocarbonyl species form two distinct bands at 2161/2147 and 2159/2151 cm^{-1}. These two separate bands have previously been correlated in literature to two structurally distinct Cu-sites [37, 38]. Cu^{I}-BEA seems to have fewer accessible Cu-sites, as shown by the lower intensity for the monocarbonyl bands for this material than the corresponding band(s) for the other zeolites. This is also corroborated by the appearance of the band at 2143 cm^{-1} at high coverages for the Cu^{I}-BEA sample, since this is the vibrational frequency of gaseous CO, indicating that all possible adsorption sites are already covered. We postulate that this is related to the low Al concentration, and hence high Cu ion loading on this sample, relative to available exchange sites, resulting in the formation of copper agglomerates.

As more CO is dosed onto the samples, a band starts appearing in the 2178–2182 cm^{-1} region. This is the symmetric stretch of Cu^{I}-$(CO)_2$, and is a clear indication that dicarbonyl species are forming. For all samples, the asymmetric stretch of Cu^{I}-$(CO)_2$ is also present at lower wavenumbers (~2149–2152 cm^{-1}), although, this is distorted by a broad tail, indicating that another band is also appearing in that area. Indeed, there seems to be a band/shoulder at around 2135 cm^{-1}, which is likely due to the presence of Cu_2O nanoparticles formed during the exchange procedure [37]. The intensity of the symmetric and asymmetric stretch for Cu^{I}-$(CO)_2$ for the Cu^{I}-MOR sample was further compared to the same vibrational frequencies from CO on the 0.30Cu^{I}-MOR sample as well as a liquid ion exchanged (LIE) Cu-MOR (Cu/Al = 0.28) with the same Si/Al ratio as the MOR investigated herein, previously published by Pappas et al. [39]. A figure comparing the three samples can be found in the SI (Fig. S4). By first comparing the high and low loaded CuCl exchanged samples, it is evident the highly exchanged sample also have more available Cu^{I} to form monocarbonyl adducts, as the band intensity for monocarbonyl is higher in the Cu^{I}-MOR sample compared to 0.30Cu^{I}-MOR. However, comparing the symmetric dicarbonyl band at 2178 cm^{-1}, the two samples show approximately the same intensity, indicating that the same amount of Cu^{I}-$(CO)_2$ is formed on the two samples. It is important to note that these values are not normalized to Cu content, indicating that 0.30Cu^{I}-MOR has a higher ratio of Cu sites available for dicarbonyl formation. Even so, when comparing both samples to the LIE sample published previously by Pappas et al., it is evident that the LIE sample has markedly higher bands for the dicarbonyl adducts, even though it has the same Cu content as 0.30Cu^{I}-MOR. Higher intensities of the symmetric and asymmetric stretch for Cu^{I}-$(CO)_2$ have been previously attributed to Cu-zeolites with a larger concentration of low-coordination Cu sites, more likely to be able to activate the C-H bond in methane [40]. This indicates that the SSIE method used for the Cu^{I}-zeolites herein, yields fewer Cu sites that are in a coordination state and position preferred for reaction with methane, compared to LIE. This could partially be due to less accessibility to the sites because of nanoparticle formation blocking the pores as observed with the reduction in specific surface area for all the zeolites. Another possibility is that some of the Cu sites are coordinated to Cl, thus limiting the coordination environment available for CO and only allowing for monocarbonyl species to form. The latter can also be corroborated by the observation of $CuCl_2$ nanoparticles with XRD after testing.

3.3 Investigating the redox properties with CH_4-TPR

To further explore the propensity of the samples for reaction with methane, CH_4-TPR experiments were used. This technique probes the redox properties of the materials. FT-IR indicated the lack of Brønsted acid sites in the material, while CO adsorption showed that only some of the Cu sites were available to form dicarbonyl adducts. Such adducts have been linked to efficient methane activation [41]. With CH_4-TPR, it is possible to determine if these properties affect the reactivity of materials towards methane. Figure 4 shows the CH_4 consumption (a) and the CO_2 production (b) against temperature during CH_4-TPR over the four materials highly exchanged materials. In Fig. 4 (c) and (d), Cu^{I}-MOR is compared to 0.30Cu^{I}-MOR.

The CH_4 consumption trace obtained with this method should be considered to be only semi-quantiative, due to the quite small changes of the intensity of the methane m/z fragments. We will therefore focus on the most distinct

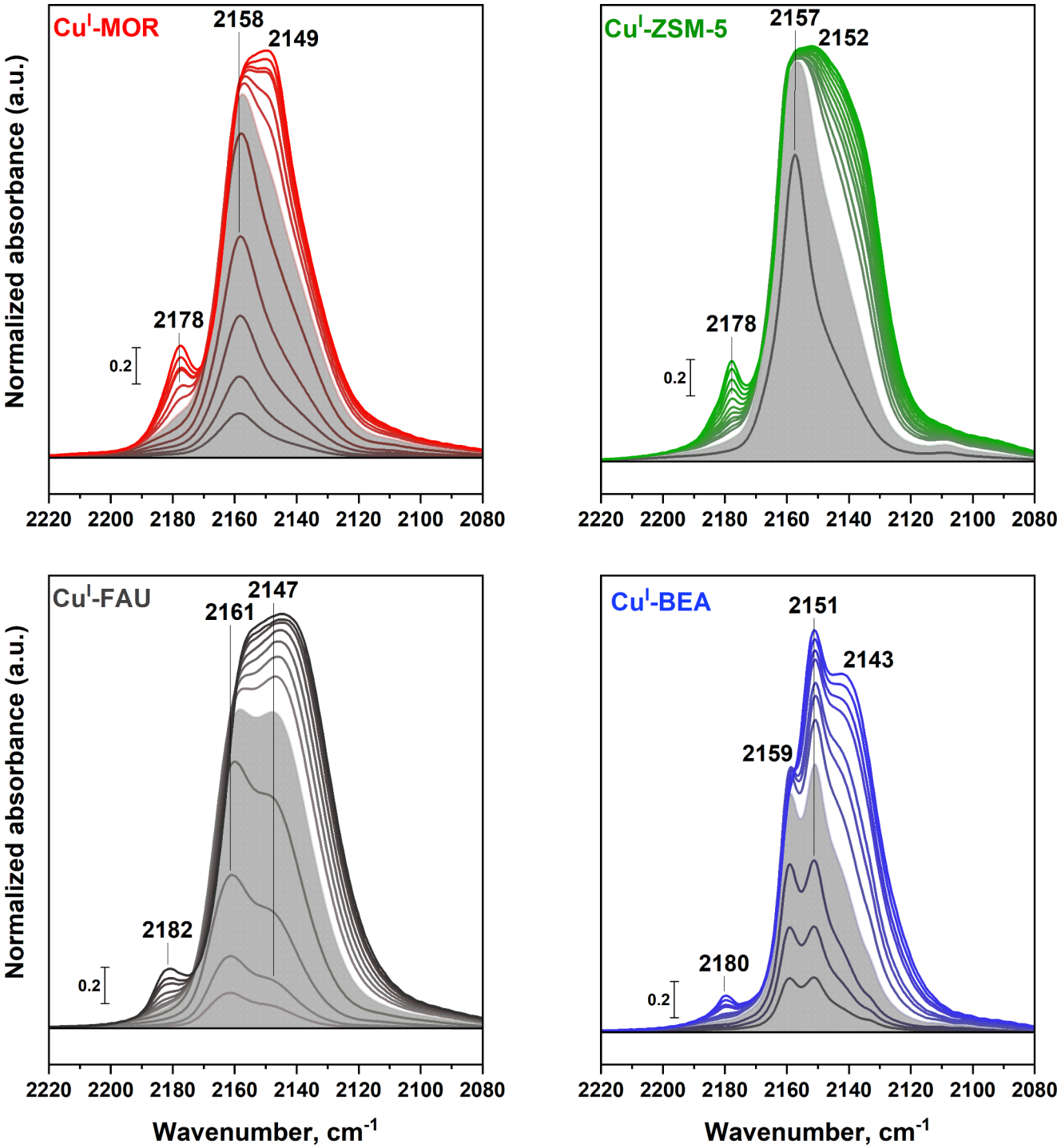

Fig. 3 FT-IR spectra showing the ν(CO) stretching region of the four Cu^{I}-zeolites during CO adsorption. The spectra have been collected with increasing CO pressure. All spectra are normalized to their framework overtone and background subtracted using the spectrum taken after pretreatment at 450 °C in vacuum. The last spectrum in all graphs is obtained after an equilibrium pressure of ca. 8 mbar was achieved. The grey area gives the last spectrum taken before the total CO pressure was large enough for dicarbonyl adducts to develop

differences that can be observed between the samples in this discussion. First, as observed in Fig. 4 (a), it is noteworthy that the onset of CH_4 consumption for the highly exchanged MOR, BEA and ZSM-5 seems to start around the same temperature, whereas the methane consumption occurs at considerably higher temperature for FAU. Further, a considerably larger quantity of methane is consumed over Cu^{I}-MOR and Cu^{I}-FAU compared to the other

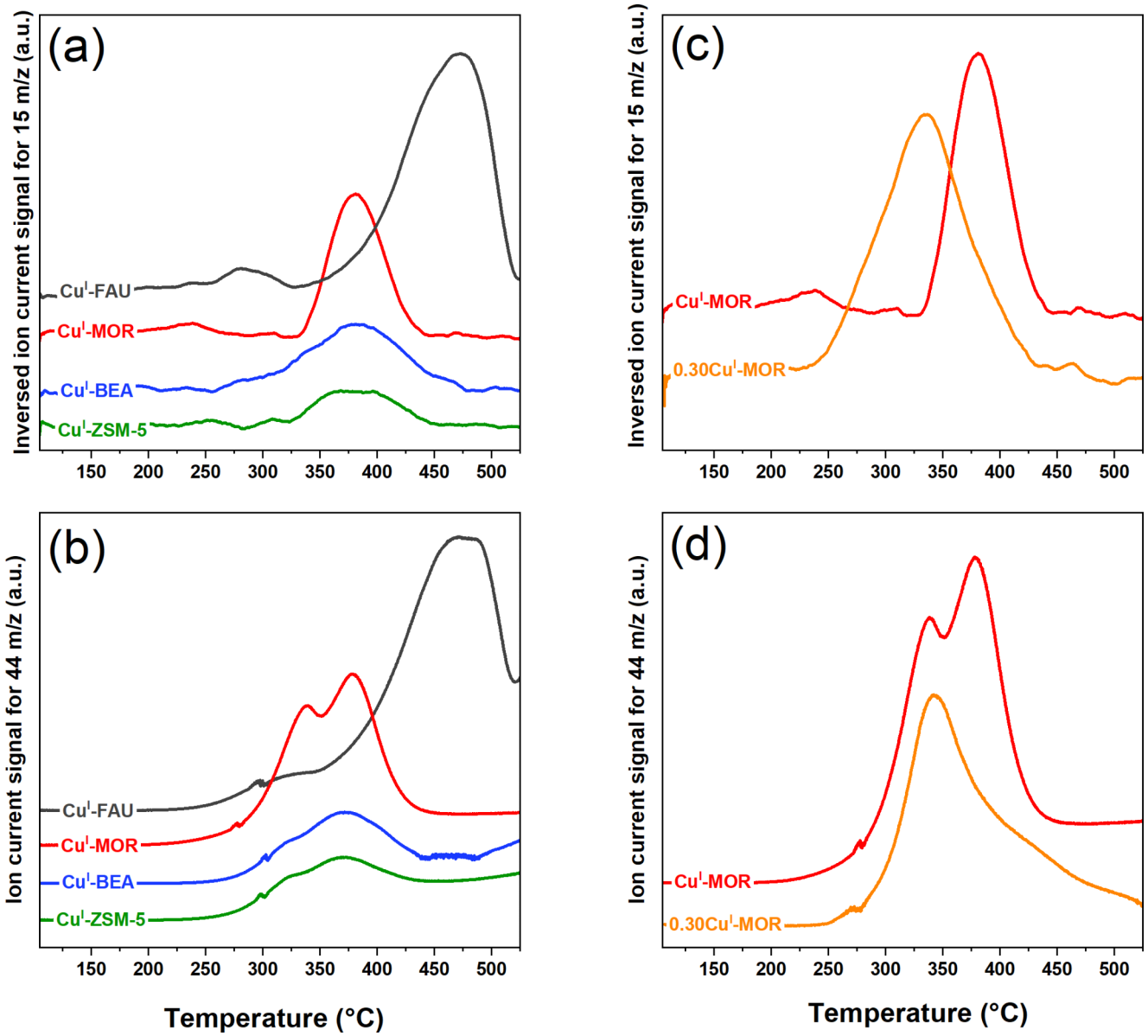

Fig. 4 CH_4-TPR signals for all four materials. On the left is the CH_4 consumption, and on the right is the corresponding CO_2 production. The graphs have been vertically adjusted for easier comparison

two materials. Sorting the materials based on the temperature of their maximum consumption rate gives Cu^{I}-ZSM-5 < Cu^{I}-MOR < Cu^{I}-BEA << Cu^{I}-FAU. This order is in line with the results previously reported by Sushkevich and van Bokhoven for CH_4 consumption on ion-exchanged Cu-zeolites [28]. When comparing the highly exchanged Cu^{I}-MOR to the 0.30Cu^{I}-MOR sample though (Fig. 4 (c)), there appears to be a significant difference in the temperature for maximum consumption rate among the two. This earlier methane consumption may suggest that 0.30Cu^{I}-MOR has a higher reactivity towards methane than Cu^{I}-MOR, likely coming from more accessible Cu_xO_y-sites.

When inspecting the CO_2 production (Fig. 4 (b) and (d)), it should be remarked that 0.30Cu^{I}-MOR, Cu^{I}-MOR and Cu^{I}-FAU produce more CO_2 than the other zeolites. The CO_2 production is also shifted to higher temperatures for FAU, in line with the higher temperature onset for CH_4 consumption. Sushkevich and van Bokhoven correlated the temperature difference for Cu-FAU to a higher fraction of monomeric Cu active sites, which require a higher temperature to activate methane. Further, it can be observed that the production of CO_2 occurs as two peaks for the highly exchanged samples, especially visible for Cu^{I}-MOR. Over 0.30Cu^{I}-MOR, on the other hand, there is one main peak with just a broad shoulder towards higher temperatures. For

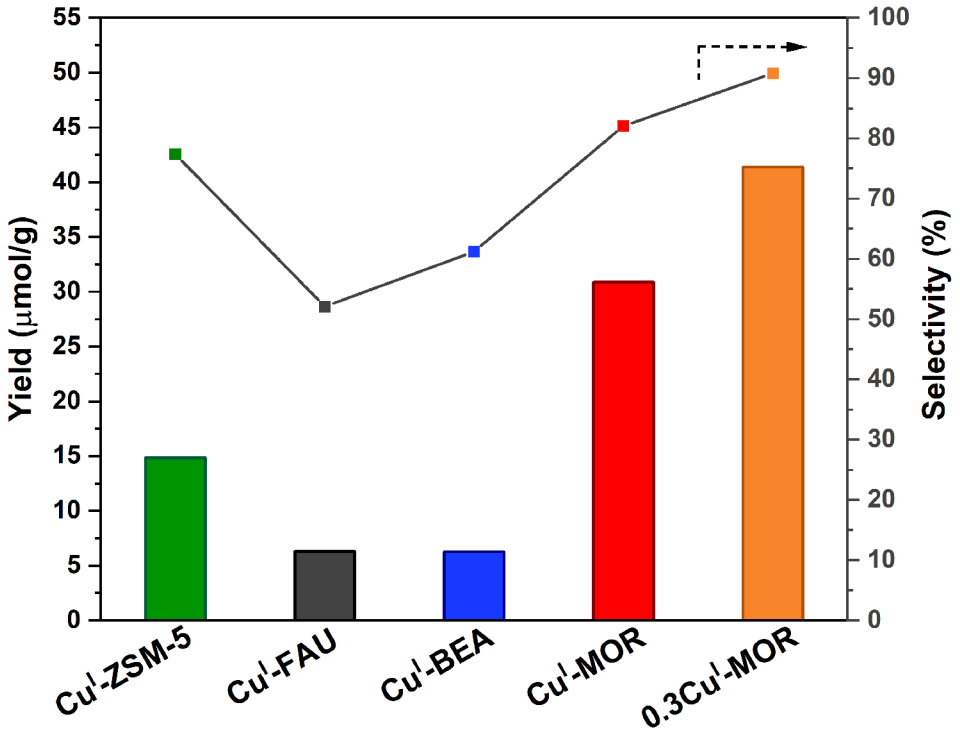

Fig. 5 Activity data for the methane to methanol reaction over the Cu^{I}-zeolites. The left axis gives the yield in μmol of total amount of methanol per gram of zeolite. On the right axis is the selectivity. In the reaction protocol, the materials were exposed to the following gas flows (15 ml/min) and temperatures; 100% O_2 (500 °C, 8 h), 100% He (200 °C, 1 h), and then, isothermally, 100% CH_4 (3 h), 100% He (1 h), and 10% H_2O in 10% Ne/He (~2 h)

the highly exchanged sample, it does appear as if the onset of CO_2 release occurs before appreciable methane consumption. However, as pointed out above, the true starting point for the uptake of CH_4 is very difficult to determine precisely. The first CO_2 peak appears at around 320 °C for all samples. As this is the main peak in 0.30Cu^{I}-MOR, the sample with the least Cu agglomerates and nanoparticles, it is likely that this is the temperature corresponding to the products formed from selective C-H activation at the active Cu-sites. Alternatively, it could be suggested that since there is a shift of methane consumption to higher temperatures for the Cu^{I}-MOR vs. 0.30Cu^{I}-MOR, the second CO_2 peak for the highly exchanged samples, which overlays well with their CH_4 consumption, is actually the one linked to CH_4 oxidation over the active Cu-sites for these species. If this is the case, it could indicate that the higher Cu-loading has led to more monomeric Cu active sites, also for the other zeolites, and not only FAU. A similar effect with methane consumption being at higher temperatures due to different framework properties was also shown comparing two different CHA frameworks (SAPO-34 vs. SSZ-13) in a previous publication by Kvande et al. [27]. Another possibility is that the higher amount of Brønsted sites in 0.30Cu^{I}-MOR aids in the reactivity towards methane, and that this is the reason behind the clear difference in CH_4 consumption temperature between the two MOR we observe herein, and not necessarily the formation of different types of Cu-oxo sites. Since it has been shown previously that Brønsted sites are important for stabilizing the methoxy intermediates, this is a plausible scenario [30].

3.4 Performance studies in the methane to methanol reaction

The propensity of Cu^{I}-zeolites (Cu^{I}-ZSM-5, Cu^{I}-FAU, Cu^{I}-BEA, Cu^{I}-MOR) towards producing methanol from methane was investigated by performing a well-established stepwise reaction protocol [7]. The test results on the four Cu^{I}-zeolites are presented in Fig. 5 below. The yield is presented in bar columns as μmol of total amount of methanol per gram of zeolite. The squared points represent the selectivity to the total amount of methanol. The unwanted byproduct of the reaction is CO_2. It should be noted that CH_3Cl is also observed as a product from the reaction but has not been included in the quantified yield or selectivity. As mentioned previously, the Cl is a remnant from the SSIE, and from EDX analysis after testing, it was observed that a large fraction of the Cl in the framework disappeared after one test, as shown in Table S2.

Excitingly, all four samples show the ability to produce methanol, although only Cu^{I}-ZSM-5 and Cu^{I}-MOR show a selectivity towards methanol similar to that previously reported for ion-exchanged zeolites [7, 11]. The appreciable yields of methanol are somewhat surprising, considering that the FT-IR study revealed very few Brønsted sites in these materials, which have been suggested to be needed for methanol formation. Thus, the results presented here might

suggest that some Cu-species can be capable of selectively converting methane to methanol without facilitation by Brønsted sites. However, formation of some Brønsted sites during the reaction protocol cannot be ruled out. Cu^{I}-ZSM-5 and Cu^{I}-MOR also give the highest yield of methanol of the four samples, with Cu^{I}-MOR clearly outperforming the others, in line with what has been observed previously for ion exchanged materials at these reaction conditions [4, 28]. These results are also very much in line with Cu^{I}-MOR being the sample that was able to consume most methane at the lowest temperature area during TPR (Fig. 4). However, Cu-FAU also has a high consumption of methane in TPR, but this occurs at higher temperature. We note that Sushkevich and van Bokhoven were able to show that Cu-FAU yielded much higher amounts of methanol when the methane activation was performed at higher temperatures [28]. Interestingly, in the same study they obtained a higher yield for BEA compared to ZSM-5, which is opposite to the results presented herein. However, this difference could be due to several unknown factors like a difference in methane loading pressure between the two studies, or it could be the higher Si/Al for BEA in this study, as well as the large over-exchange of Cu, causing fewer accessible active sites as observed by CO-adsorption with FT-IR.

To place the yields obtained in this study into perspective, the Cu^{I}-MOR can be compared to a previous publication by Dyballa et al. [4]. There, two different commercial mordenites (Si/Al = 7 and 11) were studied, starting with both H- and Na-form. A comparison between two different Cu-loading procedures was performed, i.e. liquid ion exchange (LIE) and incipient wetness impregnation (denoted SSIE in the paper). This thorough study showed that Cu exchanged onto the H-form generated more productive materials than when the ion exchange was carried out starting with the Na-form. In addition, LIE led to better Cu-mordenites with better methanol productivity than incipient wetness impregnation. The Cu^{I}-MOR used in the present study is based on the commercial MOR, CBV21A, which is the same parent material as the material with Si/Al = 11 in the paper by Dyballa et al. [4]. When comparing the total methanol yield obtained over the Cu^{I}-MOR (38 µmol/g) to the yields obtained previously (16–169 µmol/g), it is apparent that the total methanol yield of Cu^{I}-MOR is comparable to those achieved for Cu-zeolites obtained with LIE over the Na-form. However, the large fraction of inactive Cu as presented above results in an appreciably lower methanol productivity per copper for the Cu^{I}-MOR (0.03 $mol_{methanol}/mol_{Cu}$) compared to those presented by Dyballa et al. (> 0.06). From these initial results, it is suggested that a precise method is necessary to obtain a high fraction of active sites.

To investigate if we could obtain a higher fraction of active sites, and hence increase the productivity by reducing the Cu exchange degree, a Cu^{I}-MOR with a Cu/Al ≈ 0.30 was synthesized via SSIE. Indeed, this material exhibits a higher methanol productivity (0.10 $mol_{methanol}/mol_{Cu}$) as well as a higher yield of methanol, as shown in Fig. 5. The increase can likely be attributed to the formation of less nanoparticles and Cu agglomerates. Alternatively, based on the CH_4-TPR results discussed above, one could also argue that the increased productivity is related to a higher fraction of Brønsted sites present in this sample compared to the higher Cu loaded samples. However, to unravel this question would require a more extensive study where measures are taken to minimize the presence of unwanted Cu species. Interestingly, the productivity of $0.30Cu^{I}$-MOR is within the range of the productivities obtained by Dyballa et al. (0.17–0.19) on most of the materials with Si/Al = 11. However, LIE of Cu on the H-form still generates Cu-MOR with 0.25 $mol_{methanol}/mol_{Cu}$ at comparable Cu-content, outperforming the $0.30Cu^{I}$-MOR reported here.

The $0.30Cu^{I}$-MOR sample was also tested over three repeated reaction cycles to see if the removal of Cl through CH_3Cl formation had an impact on the methanol yield by potentially freeing up Cu-sites for C-H bond activation. Only a small increase was observed (from 38 to 42 µmol/g, see Fig S5), even though a qualitative analysis of the amount of CH_3Cl formed revealed a significant reduction in the CH_3Cl production from cycle to cycle (Fig S6). Previously it has been shown that repeating the test over several cycles tends to lead to a minor increase in methanol productivity [7]. Based on this, it seems that the removal of Cl from the material does not lead to an increase in methanol productivity for the samples.

4 Conclusion

Herein an alternative approach to liquid ion exchange for introducing Cu into zeolites has been investigated in the context of selective partial methane oxidation. Extensive characterization of the Cu-zeolites suggests the solid state ion exchange (SSIE) method reported here leads to a significant fraction of Cu nanoparticles and agglomerates. This is believed to hinder the ability of the materials to effectively activate methane. However, the performance data do suggest that methanol is produced on these materials, possibly without the need of Brønsted sites, indicating that methoxy intermediates can be stabilized on other surface sites. To improve on the low methanol yields however, it is necessary with the presence of more Cu-oxo species and possibly Brønsted sites, as well as higher accessibility to all of these sites, which could be achieved with a more fine-tuned

technique. As a proof of concept, we showed that the introduction of a lower amount of Cu via SSIE does result in the formation of a higher fraction of active and accessible Cu-oxo species, more Brønsted sites and a subsequently higher methanol yield. Therefore, we believe that a SSIE method, with some reduction in the amount of Cu exchanged, and a change in Cu-source that does not lead to Cl-based byproducts, could be a viable option in the future for efficient and scalable synthesis of Cu-zeolites for the methane to methanol reaction.

Supplementary Information The online version contains supplementary material available at https://doi.org/10.1007/s11244-022-01763-7.

Funding This publication forms a part of the iCSI (industrial Catalysis Science and Innovation) Centre for Research-based Innovation, which receives financial support from the Research Council of Norway under contract no. 237922. FS, PP and SC thank the Centre National de la Recherche Scientifique (CNRS), University of Strasbourg, and the French Ministry of Research for financial support. FS also thanks the French Ministry of Research for a Ph.D. fellowship.
Open access funding provided by University of Oslo (incl Oslo University Hospital)

Declarations

Conflict of interest The authors declare no conflict of interest.

References

1. Labinger JA (2004) Selective alkane oxidation: hot and cold approaches to a hot problem. J Mol Catal A: Chem 220:27–35
2. Horn R, Schlögl R (2015) Methane activation by heterogeneous catalysis. Catal Lett 145:23–39
3. Ravi M et al (2019) Misconceptions and challenges in methane-to-methanol over transition-metal-exchanged zeolites. Nat Catal 2:485–494
4. Dyballa M et al (2019) On how copper Mordenite Properties govern the Framework Stability and Activity in the methane-to-methanol Conversion. ACS Catal 9:365–375
5. Sushkevich VL et al (2017) Selective anaerobic oxidation of methane enables direct synthesis of methanol. Science 356:523–527
6. Alayon EM et al (2012) Catalytic conversion of methane to methanol over Cu-mordenite. Chem Commun 48:404–406
7. Pappas DK et al (2017) Methane to methanol: structure-activity Relationships for Cu-CHA. J Am Chem Soc 139:14961–14975
8. Wulfers MJ et al (2015) Conversion of methane to methanol on copper-containing small-pore Zeolites and Zeotypes. Chem Commun 51:4447–4450
9. Groothaert MH et al (2005) Selective oxidation of methane by the bis(μ-oxo)dicopper core stabilized on ZSM-5 and mordenite zeolites. J Am Chem Soc 127:1394–1395
10. Woertink JS et al (2009) A $[Cu_2O]^{2+}$ Core in Cu-ZSM-5, the Active Site in the Oxidation of Methane to Methanol. Proc. Natl. Acad. Sci. USA 106:18908–18913
11. Pappas DK et al (2018) The nuclearity of the active site for methane to methanol Conversion in Cu-Mordenite: a quantitative Assessment. J Am Chem Soc 140:15270–15278
12. Prodinger S et al (2022) Synthesis–structure–activity relationship in Cu-MOR for partial methane oxidation: Al Siting via Inorganic structure-directing agents. ACS Catal 12:2166–2177
13. Knorpp AJ et al (2018) Copper-exchanged omega (MAZ) Zeolite: copper-concentration dependent active Sites and its unprecedented methane to methanol Conversion. ChemCatChem 10:5593–5596
14. Kvande K et al (2020) Advanced X-ray absorption spectroscopy analysis to Determine structure-activity Relationships for Cu-Zeolites in the Direct Conversion of methane to methanol. ChemCatChem 12:2385–2405
15. Sushkevich VL et al (2021) Identification of Kinetic and Spectroscopic Signatures of Copper Sites for Direct Oxidation of methane to methanol. Angew Chem Int Ed Engl 60:15944–15953
16. Dinh KT et al (2019) Continuous partial oxidation of methane to methanol catalyzed by diffusion-paired copper dimers in copper-exchanged Zeolites. J Am Chem Soc 141:11641–11650
17. Vennestrøm PNR et al (2014) Influence of lattice stability on hydrothermal deactivation of Cu-ZSM-5 and Cu-IM-5 zeolites for selective catalytic reduction of NOx by NH3. J Catal 309:477–490
18. Shwan S et al (2015) Solid-state ion-exchange of copper into Zeolites facilitated by Ammonia at Low Temperature. ACS Catal 5:16–19
19. Le HV et al (2017) Solid-state ion-exchanged Cu/Mordenite catalysts for the Direct Conversion of methane to methanol. ACS Catal 7:1403–1412
20. Bozbag SE et al (2016) Methane to methanol over copper Mordenite: yield improvement through multiple cycles and different synthesis techniques. Catal Sci Technol 6:5011–5022
21. Kuhn P et al (2009) Probing Cu-USY Zeolite Reactivity: design of a Green Catalyst for the synthesis of Diynes. J Phys Chem C 113:2903–2910
22. Chassaing S et al (2017) Zeolites as Green Catalysts for Organic synthesis: the cases of H-, Cu- & Sc-Zeolites. Curr Org Chem 21:779–793
23. Chassaing S et al (2018) Green catalysts based on zeolites for heterocycle synthesis. Curr Opin Green Sustainable Chem 10:35–39
24. Clerc A et al (2020) Chan-Lam-type azidation and One-Pot CuAAC under CuI-Zeolite Catalysis. ChemCatChem 12:2060–2065
25. Schlimpen F et al (2022) From A3/KA2 to AYA/KYA multicomponent coupling reactions with terminal ynamides as alkyne surrogates – a direct, green route to γ-amino-ynamides. Green Chem 24:6467–6475
26. Schlimpen F et al (2021) α-Tertiary propargylamine synthesis via KA2-Type coupling reactions under Solvent-Free CuI-Zeolite Catalysis. J Org Chem 86:16593–16613
27. Kvande K et al (2020) Comparing the nature of active Sites in Cu-loaded SAPO-34 and SSZ-13 for the Direct Conversion of methane to methanol. Catalysts 10:191

28. Sushkevich VL, van Bokhoven JA (2019) Methane-to-Methanol: activity descriptors in copper-exchanged Zeolites for the Rational design of materials. ACS Catal 9:6293–6304
29. Llewellyn P et al (2006) Characterization of porous solids VII. Stud Surf Sci Catalysis; Elsevier 160:748
30. Dyballa M et al (2019) Zeolite Surface Methoxy Groups as Key Intermediates in the Stepwise Conversion of methane to methanol. ChemCatChem 11:5022–5026
31. Sushkevich VL et al (2020) Pathways of Methane Transformation over copper-exchanged Mordenite as revealed by In-Situ NMR and IR Spectroscopy. Angew Chem Int Ed 59:910–918
32. Alayon EMC et al (2015) Bis(μ-oxo) Versus mono(μ-oxo) dicopper cores in a Zeolite for converting methane to methanol: an *in situ* XAS and DFT Investigation. Phys Chem Chem Phys 17:7681–7693
33. Borfecchia E et al (2015) Revisiting the nature of Cu sites in the activated Cu-SSZ-13 Catalyst for SCR reaction. Chem Sci 6:548–563
34. Larsen SC et al (1994) Electron Paramagnetic Resonance Studies of Copper Ion-Exchanged ZSM-5. J Phys Chem 98:11533–11540
35. Llabrés i Xamena FX et al (2003) Thermal reduction of Cu^{2+}–Mordenite and Re-oxidation upon Interaction with H_2O, O_2, and NO. J Phys Chem B 107:7036–7044
36. Sushkevich VL, van Bokhoven JA (2018) Revisiting copper reduction in zeolites: the impact of autoreduction and sample synthesis procedure. Chem Commun 54:7447–7450
37. Giordanino F et al (2013) Characterization of Cu-Exchanged SSZ-13: a comparative FTIR, UV-Vis, and EPR Study with Cu-ZSM-5 and Cu-beta with similar Si/Al and Cu/Al Ratios. Dalton Trans 42:12741–12761
38. Palomino GT et al (2000) XRD, XAS, and IR characterization of copper-exchanged Y Zeolite. J Phys Chem B 104:8641–8651
39. Pappas DK et al (2021) Influence of Cu-speciation in mordenite on direct methane to methanol conversion: Multi-Technique characterization and comparison with NH3 selective catalytic reduction of NOx. Catal Today 369:105–111
40. Pappas DK et al (2019) Understanding and optimizing the performance of Cu-FER for the direct CH_4 to CH_3OH Conversion. ChemCatChem 11:621–627
41. Palomino GT et al (2002) Vibrational and optical spectroscopic studies on copper-exchanged ferrierite. Stud Surf Sci Catal 142:199–206